Separation and Purification Technology 298 (2022) 121604

Contents lists available at ScienceDirect

Separation and Purification Technology

journal homepage: www.elsevier.com/locate/seppur

Ni/support-CaO bifunctional combined materials for integrated CO_2 capture and reverse water-gas shift reaction: Influence of different supports

Shuzhuang Sun [a], Chen Zhang [a], Shaoliang Guan [b,c], Shaojun Xu [b,d,*], Paul T. Williams [e,*], Chunfei Wu [a,*]

[a] School of Chemistry and Chemical Engineering, Queen's University Belfast, Belfast BT7 1NN, UK
[b] Cardiff Catalysis Institute, School of Chemistry, Cardiff University, Cardiff CF10 3AT, UK
[c] Harwell XPS, Research Complex at Harwell, Rutherford Appleton Laboratory, Didcot OX11 0FA, UK
[d] UK Catalysis Hub, Research Complex at Harwell, Didcot OX11 0FA, UK
[e] School of Chemical and Process Engineering, University of Leeds, Leeds LS2 9JT, UK

ARTICLE INFO

Keywords:
Integrated CO_2 capture and utilisation
Reverse water-gas shift reaction
Bifunctional combined materials

ABSTRACT

Integrated CO_2 capture and utilisation (ICCU) is a promising strategy for restricting carbon emissions and achieving carbon neutrality. Bifunctional combined materials (BCMs), containing adsorbents and active catalysts, are widely applied in this process. Producing syngas via reverse water–gas shift reaction (RWGS) and integrating with Fischer-Tropsch (F-T) synthesis is an attractive and valuable CO_2 utilisation route. This work investigated a series of Ni/support-CaO BCMs (supports = ZrO_2, TiO_2, CeO_2 and Al_2O_3) for the integrated CO_2 capture and RWGS (ICCU-RWGS) process. The Ni/support-CaO BCMs were prepared by physically mixing various metal oxide supports loaded Ni with sol–gel derived CaO. The ICCU-RWGS performance (CO_2 conversion, CO yield and CO generation rate) of these BCMs followed the order during tested conditions (550–750 °C): Ni/CeO_2-CaO > Ni/TiO_2-CaO > Ni/ZrO_2-CaO > Ni/Al_2O_3-CaO. A comprehensive characterisation of Ni/support materials showed that Ni/CeO_2 had the characteristics of stronger basicity, optimal Ni dispersion and improved NiO reducibility, which led to the outperforming ICCU-RWGS activity over Ni/CeO_2-CaO (e.g. 56.1% CO_2 conversion, 2.68 mmol g^{-1} CO yield and ~100% CO selectivity at 650 °C). Furthermore, the Ni/CeO_2-CaO BCM showed a stable, yet, self-optimising catalytic performance during the cyclic ICCU-RWGS reaction over 20 cycles. The TEM characterisation suggested that was ascribed to the volume expansion and shrinkage of CaO in the cyclic adsorption–desorption altering the distance between the adsorbent and Ni/CeO_2, resulting in an enhanced CO_2 conversion during the cycle.

1. Introduction

With the wide use of fossil fuels, a substantial amount of CO_2 emissions is emitted into the atmosphere, leading to severe environmental issues [1], such as sea level rise [2], ocean acidification [3] and extreme weather [4]. In order to reduce industrial carbon emissions, CO_2 capture is one of the most promising techniques and has attached a lot of attention [5–8]. Currently, the most mature CO_2 capture technologies are solvents adsorption (i.e. MEA) [9] and calcium looping [10–13], which are both operated by swinging temperature to regenerate the adsorbents. The obtained high concentration of CO_2 could be stored by deep-sea injection or mineralisation [14], which is known as carbon capture and storage (CCS). However, the CCS requests a high capital investment and may not be a long-term sustainable solution due to the risk of the second release of stored CO_2 [15]. Therefore, there is an increasing interest in the direct utilisation of the captured CO_2, which is known as integrated CO_2 capture and utilisation (ICCU).

The ICCU process can eliminate the CO_2 enrichment, storage and transportation steps by in-situ converting the captured CO_2 [16] and isothermally producing valuable products (e.g. CH_4 or CO [17–20]). In a typical ICCU process, CO_2 is first adsorbed on adsorbents (i.e. CaO), and then a reducing agent (i.e. H_2) is introduced to react with the captured CO_2 with the assistance of active catalytic sites. Among the final products of the ICCU process, carbon monoxide (CO) is considered to be one of the most valuable chemicals to be used as the feedstock for the mature Fischer-Tropsch process to further produce liquid products [21–23]. The

* Corresponding authors.
E-mail addresses: xus25@cardiff.ac.uk (S. Xu), p.t.williams@leeds.ac.uk (P.T. Williams), c.wu@qub.ac.uk (C. Wu).

https://doi.org/10.1016/j.seppur.2022.121604
Received 24 May 2022; Received in revised form 22 June 2022; Accepted 25 June 2022
Available online 28 June 2022

commonly used CO_2 reduction technologies include thermal-catalysis, photo-catalysis, electro-catalysis, plasma-catalysis and etc. [24]. Thermal-catalyzed CO_2 reduction is a relatively compromised choice in terms of high process efficiency and low input cost (e.g. equipment investment and materials costs). The reverse water–gas shift (RWGS) reaction, as shown in Eq. (1), is a promising process for thermal catalytic conversion of CO_2 that uses renewable H_2 to reduce carbon emissions and produce syngas.

$$CO_2 + H_2 = CO + H_2O \tag{1}$$

The bifunctional combined materials (BCMs), containing CO_2 adsorbent and active catalytic sites, have been proven effective for the ICCU process [20,23,25–27]. Specifically, CaO is widely used as high temperature CO_2 adsorbent [28,29], and Ni can act as catalytic sites for RWGS [30,31]. The previous study [32] has concluded that the physical mixing is a superior material preparation method by avoiding catalytic sites coverage due to CaO sintering. The supports of Ni-catalysts are widely believed to play key roles in the catalytic process owing to the metal dispersion, metal-support interaction, etc. [33–35]. However, as a novel process, ICCU provide CO_2 in the form of carbonates, which possesses different chemical environment than traditional RWGS. Therefore, there is a gap on understanding of the effects of supports in ICCU, including the effects on CO_2 adsorption and catalytic conversion.

In this work, to investigate the support effects on ICCU-RWGS, two active supports (CeO_2 and TiO_2) and inert materials (ZrO_2 and Al_2O_3) supported Ni are synthesised as catalysts, and a sol–gel prepared CaO as the adsorbent to prepare the BCMs. The sol–gel CaO has been proven a stable and excellent CO_2 adsorbent in carbon capture [36]. The CeO_2 and TiO_2 have been widely applied to catalytic processes, including RWGS, CO_2 methanation, dry reforming etc. [37,38]. Furthermore, the active TiO_2 and inert Al_2O_3 could form spinel with Ni (strong metal-support interaction) [39,40], which provide valuable benchmarks for identifying active sites.

2. Experimental section

2.1. Bifunctional combined materials preparation

ZrO_2 (Sigma-Aldrich, 99%), TiO_2 (Sigma-Aldrich, 99.5%) and Al_2O_3 (Sigma-Aldrich, 99.5%) were dried at 120 °C before the impregnation process. CeO_2 was prepared by a hydrothermal method as reported in previous work [17,19]. Briefly, 5.21 g $Ce(NO_3)_3{\cdot}6H_2O$ (Sigma-Aldrich, 99%) was dissolved in deionised water (30 ml) to prepare a Ce source solution, followed by the dissolution of 57.6 g NaOH (Sigma-Aldrich, 99%) in deionised water (210 ml) to prepare the precipitant. The Ce source was mixed with the precipitant dropwise for 30 mins at room temperature to obtain a slurry. The slurry was transferred into a stainless-steel autoclave and kept at 100 °C for 24 h. The precipitate was washed and separated by vacuum filtration using distilled water and ethanol to neutrality and dried at 120 °C overnight, to produce a yellow powder, labeled as CeO_2. Ni-based catalysts were prepared by the wet impregnation method, using $Ni(NO_3)_2{\cdot}6H_2O$ (Sigma-Aldrich, 97%) as the metal precursor. Typically, 3.0 g support material was added into 30 ml $Ni(NO_3)_2$ (0.15 mol L^{-1}) aqueous solution, stirred at room temperature for 2 h and evaporated under stirring to produce a sample paste. The sample paste was dried at 120 °C overnight, and calcined at 800 °C for 5 h with a heating rate of 5 °C min^{-1}, to produce NiO/ZrO_2, NiO/TiO_2, NiO/CeO_2 and NiO/Al_2O_3, respectively. The NiO/supports were reduced at 550 °C for 2 h with a heating rate of 5 °C min^{-1} in 5% H_2/N_2, and labeled as Ni/ZrO_2, Ni/TiO_2, Ni/CeO_2 and Ni/Al_2O_3, respectively.

The sol–gel derived CaO was prepared as reported in previous work [20,32]. Briefly, 23.6 g $Ca(NO_3)_2{\cdot}4H_2O$ (Sigma-Aldrich, 99%) and 19.2 g citric acid monohydrate (Sigma-Aldrich, 99.5%) were dissolved into 72 ml distilled water, stirred at room temperature at 80 °C, and dried at 120 °C overnight. The sample was ground and calcined at 850 °C for 5 h with a heating rate of 5 °C min^{-1}, labeled as sol–gel CaO. The bifunctional combined materials were prepared by physically mixing the Ni/support catalysts and the sol–gel CaO with a mass ratio of 1:2, labeled as Ni/ZrO_2-CaO, Ni/TiO_2-CaO, Ni/CeO_2-CaO and Ni/Al_2O_3-CaO, respectively.

2.2. Materials characterisation

The loadings of Ni on various supports were measured by inductively coupled plasma-optical emission spectroscopy (ICP-OES). The samples were digested in nitric acid and then analysed using a Perkin Elmer PE2400 CHNS. X-ray diffraction (XRD) patterns (2 Theta: 5°-75°) were measured by a PANalytical Empyrean Series 2 diffractometer with a Cu Ka X-ray source. The surface area and pore structure of the Ni/supports catalysts were characterised by an ASAP 3000 analyser at 77 K. The Brunauer-Emmett-Teller (BET) method and the desorption isotherm branch were applied to calculate the surface area and the pore size distribution, respectively. The X-ray photoelectron spectrum (XPS) analysis was performed on a Thermo Fisher Scientific NEXSA spectrometer. H_2 temperature-programmed reduction (H_2-TPR) of the NiO/support catalysts was tested on a Hi-Res TGA 2950 thermogravimetric analyser. Typically, the samples were pre-treated under N_2 at 300 °C for 30 mins to remove the adsorbed H_2O and gases, equilibrated to 50 °C and temperature programmed reduced in 100 ml min^{-1} 5% H_2/N_2 (10 °C/min to 800 °C). The CO_2 temperature-programmed desorption (CO_2-TPD) patterns of the Ni/support catalysts were measured by a Micromeritics Autochem II 2920 analyser. The Ni/support catalysts were *in-situ* reduced at 550 °C in H_2 for 1 h and then cooled down to 30 °C in He. After adsorbing CO_2 at 30 °C in 10% CO_2/He, the temperature was increased to 800 °C in He with a heating rate of 10 °C min^{-1}. Scanning electron microscopy coupled with an energy dispersive X-ray spectrometer (SEM-EDX, FEI Quanta FEG) was used to characterise the morphology and element dispersion. Transmission electron microscopy (TEM, FEI Titan3 Themis 300) and high-angle annular dark-field transmission electron microscopy (HAADF-TEM) were utilised to observe the morphology and Ni particle size of Ni/support catalysts. The Ni particle size distribution was calculated from TEM observation.

2.3. Integrated CO_2 capture and RWGS (ICCU-RWGS) evaluation studies

The ICCU-RWGS evaluations of Ni/support-CaO were carried out in a fixed-bed reactor and monitored by an online gas analyser (Kane Autoplus 5). The stainless-steel reaction tube (length: 500 mm, inner diameter: 64 mm) was placed in the middle of the tube furnace (Elite TSH-2416CG). Briefly, 0.30 g Ni/support-CaO bifunctional combined materials (BCMs) were placed in the middle of the reaction tube and fixed in place by quartz wool. Two thermocouples were placed in the reaction tube and inside the tube furnace to monitor the temperature of the BCMs and tube furnace, respectively.

In a typical evaluation test, the BCMs were reduced at 550 °C in 5% H_2/N_2 for 2 h, and then the gas was switched to 100 ml min^{-1} 20% CO_2/N_2 for ~28 mins. 100 ml min^{-1} 5% H_2/N_2 was then introduced for ~28 mins for the RWGS. Then the flowing gas was switched to N_2 and equilibrated the temperature for the following test. The baseline of carbonation and hydrogenation steps was monitored using 0.3 g SiO_2 to eliminate the analyser signal delay. The CO_2 conversion, CO yield and selectivity were calculated by integrating the real-time data collected from the online gas analyser from 0 s to 1700 s, referring to the equations below.

$$C_{CO2} = \frac{\int_0^{1700}(CO + CH_4)}{\int_0^{1700}(CO + CH_4 + CO_2)} *\% \tag{2}$$

Table 1
Summary of element analysis, BET, pore size and average Ni crystallite size.

Sample	Ni content[a] (wt. %)	S_{BET}[b] (m^2 g^{-1})	V_{pore}[c] (m^3 g^{-1})	Average pore size (nm)	Ni crystallite size[d] (nm)
Ni/ZrO_2	7.8	4.7	0.1	21.1	34.1
Ni/TiO_2	9.5	3.5	0.1	23.7	27.9
Ni/CeO_2	6.8	63.9	0.3	17.7	18.7
Ni/Al_2O_3	8.1	126.3	0.2	5.1	21.3
Sol-gel CaO	–	9.4	0.1	35.9	–

[a] Element percentage evaluated by elemental analysis.
[b] Multipoint BET surface area.
[c] BJH method cumulative desorption pore volume.
[d] Average Ni crystallite sizes calculated from XRD.

$$S_{CO} = \frac{\int_0^{1700} CO}{\int_0^{1700}(CO + CH_4)} *\% \quad (3)$$

$$Y_{CO} = \frac{\int_0^{1700} CO(\%*s)*1.667(ml/s)}{22.4(ml/mmol)*0.30(g)} \quad (4)$$

C_{CO2}, S_{CO} and Y_{CO} represent to CO_2 conversion (%), CO selectivity (%) and CO yield (mmol $g^{-1}_{material}$).

3. Results and discussion

3.1. Characterisation of Ni/support catalysts and Ni/support-CaO bifunctional combined materials

3.1.1. Ni/support catalysts

The elemental analysis of the Ni/support catalysts using inductively coupled plasma (ICP) showed that the Ni loadings on the various supports were controlled at 8 ± 1.5 wt% (Table 1). N_2 isothermal adsorption–desorption was carried out to characterise the surface area and pore structure of the Ni/support materials (Fig. 1). As summarised in Table 1, the Ni/ZrO_2 and Ni/TiO_2 showed poor porosity with low BET surface areas (< 5 m^2 g^{-1}). In contrast, the Ni/CeO_2 and Ni/Al_2O_3 were more porous and possessed typical type IV isotherms with distinct hysteresis loops. As shown in Fig. 1, the Ni/CeO_2 and Ni/Al_2O_3 exhibited type H_3 and H_4 hysteresis loops with various pore size distribution. The pore size of Ni/CeO_2 and Ni/Al_2O_3 are ~10–40 nm and 3–10 nm, respectively. It can also be demonstrated from TEM observation (Fig. 2i) that Ni/CeO_2 could accumulate slit-shaped pores with regular rod-like morphology. The higher surface area and porous structure could contribute to the dispersion of metals and the diffusion of reactants in catalytic reactions.

High-angle annular dark-field transmission electron microscopy (HAADF-TEM) was carried out to observe the dispersion of Ni species and the morphologies of the Ni/support catalysts. As shown in Fig. 2, all the Ni/support catalysts possessed gaussian distribution of Ni species size, following the decreasing order: Ni/TiO_2 > Ni/ZrO_2 > Ni/Al_2O_3 > Ni/CeO_2. The Ni species size distribution and the average Ni size are presented in Fig. 2d, h, l, p. The CeO_2 and Al_2O_3 can disperse Ni better than other supports, which is attributed to the morphology and porosity of supports. Specifically, the Ni/CeO_2 possesses the optimal Ni dispersion with a ~14.1 nm Ni species size.

The X-ray diffraction patterns of the Ni/support materials are presented in Fig. 3. Except for the amorphous Al_2O_3 supported Ni, all the other three samples showed distinct metallic Ni peaks (PDF#87-0712) and strong diffraction peaks which belong to the support materials, referring to ZrO_2 (PDF#86-1451), TiO_2 (PDF#75-1753) and CeO_2 (PDF#78-0694). In addition, the Ni/TiO_2 and Ni/Al_2O_3 catalysts exhibited $NiTiO_3$ (PDF#76-0334) and $NiAl_2O_4$ (PDF#77-1877) spinel peaks, respectively. There were no distinct NiO peaks, indicating that NiO was fully reduced at 550 °C during the reduction process. The reducibility of spinel is much poorer than NiO species [41,42], which could be verified by the presence of significant spinel peaks after reduction.

XPS was carried out, as shown in Fig. 4, to further confirm the valence state and chemical environment of surface nickel species of the reduced Ni/support catalysts. The Ni $2p_{3/2}$ XPS profiles of Ni/supports exhibit common peaks at ~852.1 eV and ~855.8 eV, which are attributed to the metallic Ni and its satellite peak, respectively [43]. The air contact could quickly oxidise surface metallic Ni, resulting in the existence Ni^{2+} peaks on the reduced Ni/support catalysts [44]. The multi-split peaks at 853.5–855.5 eV and 857–861 eV could be assigned as Ni^{2+} signals from NiO and their satellite peaks. Notably, there is no distinct NiO peaks on XRD characterisations (Fig. 3), indicating the oxidation only limitedly occurs on the surface of Ni. It is believed that the support interacted Ni would possess higher binding energy [45], which can be located at 856.5 eV and 862.3 eV. Notably, the Ni/Al_2O_3 possessed the most abundant metal-support interaction, indicating that the $NiAl_2O_4$ dominates on the surface of Ni/Al_2O_3 [39]. As a comparison, the surface $NiTiO_3$ could be effectively reduced and exhibited ~34% Ni^0 even after air oxidation. It is noted that $NiTiO_3$ still dominate in bulk (Fig. 3), indicating that the Ni might parse out from $NiTiO_3$

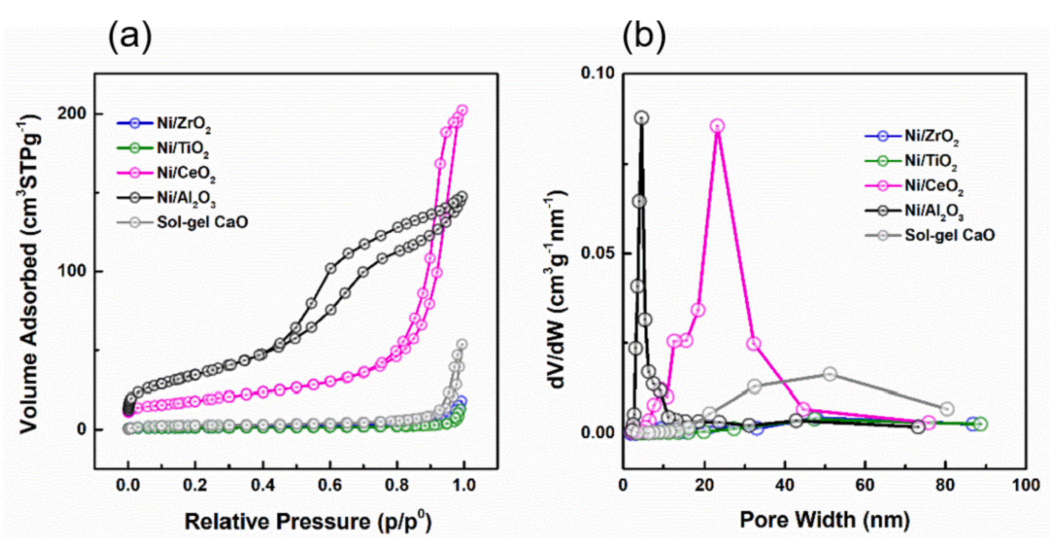

Fig. 1. (a) N_2 adsorption–desorption isotherms; (b) Pore size distribution calculated from the BJH desorption branch.

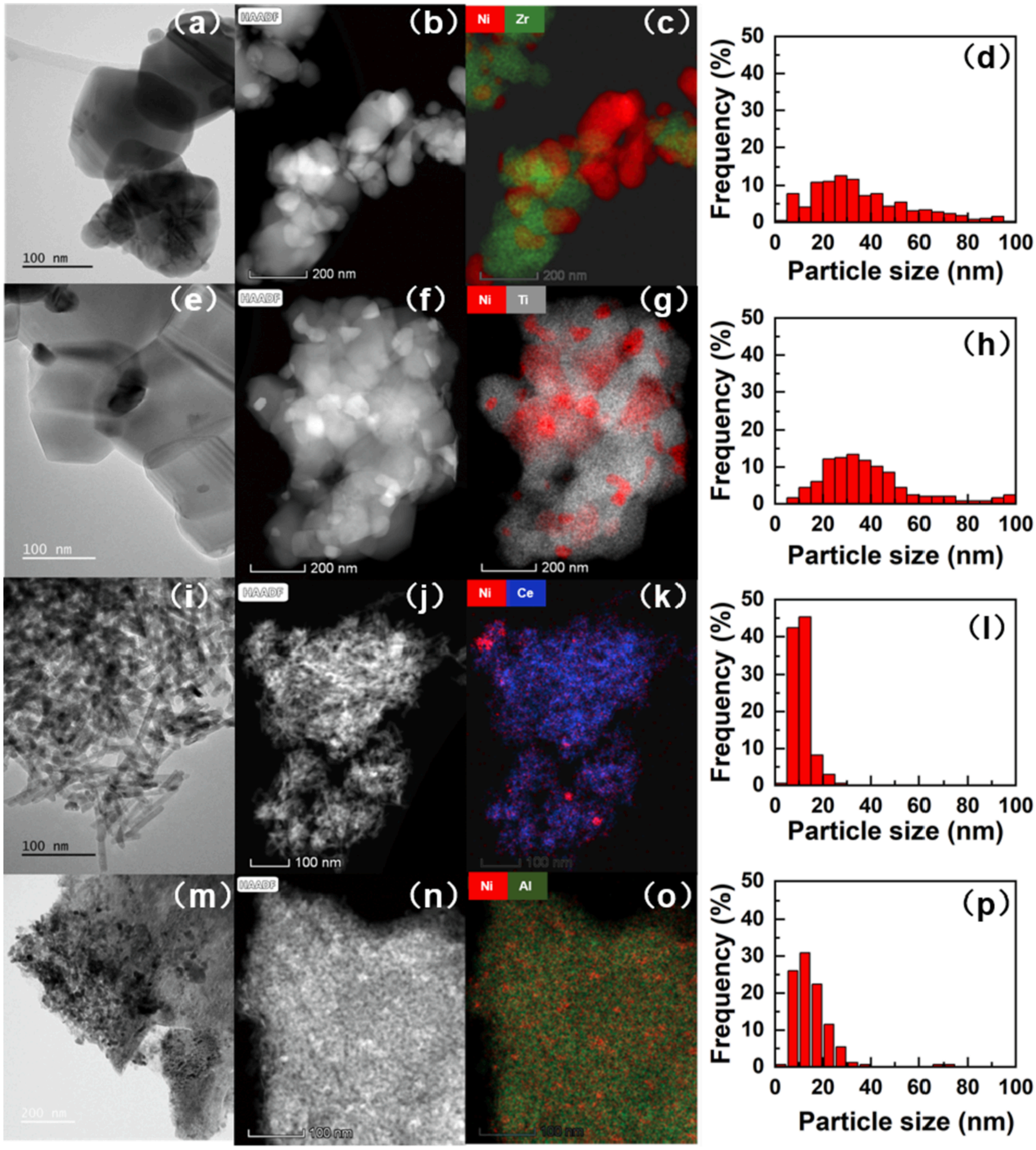

Fig. 2. TEM, HAADF-mapping images and Ni size distribution of Ni/support catalysts. (Ni/ZrO_2: a, b, c and d; Ni/TiO_2: e, f, g and h; Ni/CeO_2: i, j, k and l; Ni/Al_2O_3: m, n, o and p).

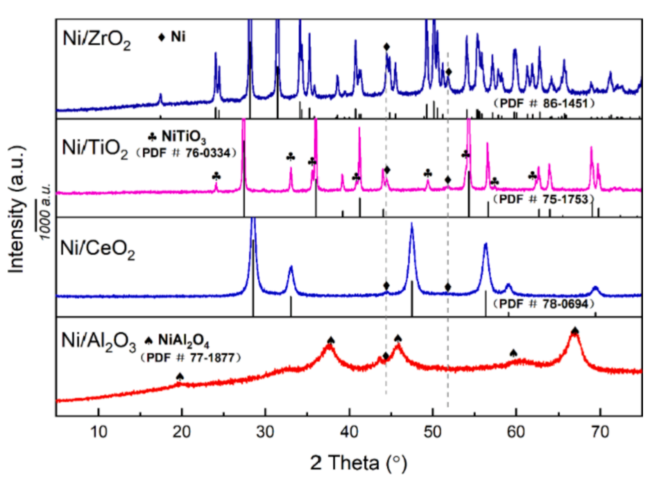

Fig. 3. XRD patterns of Ni/support catalysts with various supports (ZrO_2, TiO_2, CeO_2 and Al_2O_3).

spinel and act as catalytic sites in ICCU. The Ni/CeO_2 exhibits lower metallic Ni fraction (18%) on the surface, attributed to the highly dispersed Ni, which could be easily reacted with O_2 in air.

The reducibility of the Ni species over the prepared NiO/support catalysts was further investigated by H_2-TPR, as shown in Fig. 5a. There are two reduction peaks over Ni/ZrO_2 and Ni/CeO_2 at 380–430 °C and 450–480 °C, which could be assigned as weakly and strongly interacted NiO species, respectively [41,46]. It is noted that the NiO/CeO_2 possessed the lowest reduction temperature, which is attributed to the smallest Ni particle size [47]. The spinel species (i.e. $NiAl_2O_4$ and $NiTiO_3$) formed during the high temperature calcination are more difficult to reduce, which is consistent with the XRD analysis. Specifically, the $NiTiO_3$ spinel can be reduced from ~600 °C and showed only one reduction peak at ~680 °C [41]. And there was no distinct reduction of Ni/Al_2O_3 in the TPR procedure [42]. The formation of spinel is believed to improve Ni dispersion [23],[48]; however, only the reducible Ni species are active catalytic sites.

CO_2-TPD profiles are presented in Fig. 5b to investigate the basicity of the Ni/support catalysts. Only Ni/CeO_2 and Ni/Al_2O_3 possessed CO_2

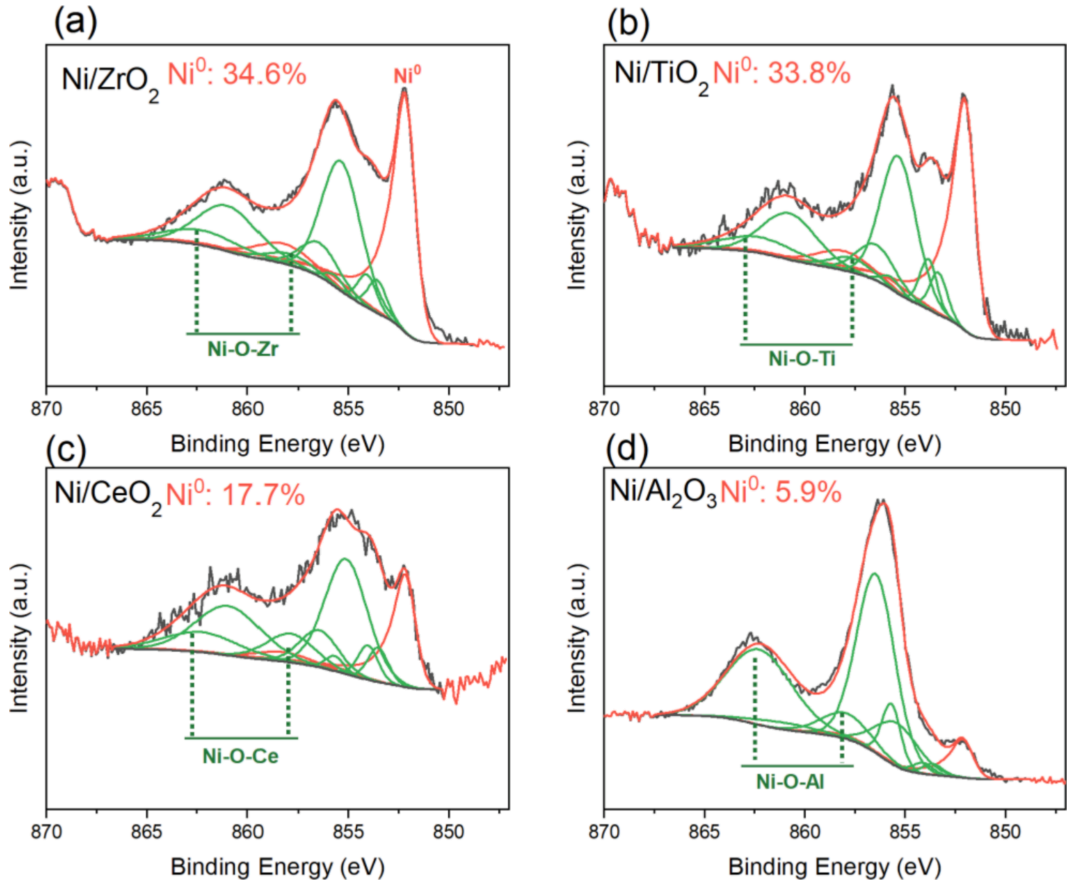

Fig. 4. XPS analysis of Ni $2p_{3/2}$ region of (a) Ni/ZrO_2; (b) Ni/TiO_2; (c) Ni/CeO_2 and (d) Ni/Al_2O_3.

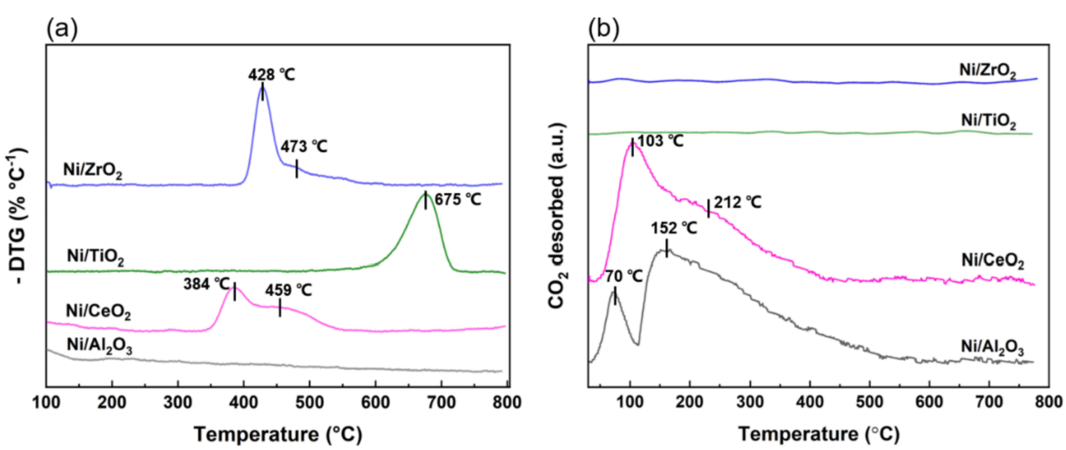

Fig. 5. (a) H_2-TPR patterns of NiO/support catalysts and (b) CO_2-TPD patterns of Ni/support catalysts.

desorption peaks, which are attributed to their surface basic sites and superior porosity. The two desorption peaks of Ni/CeO_2 and Ni/Al_2O_3 at temperatures of < 100 °C and between 150 and 250 °C are attributed to weak and intermediate CO_2 chemisorption, respectively [49]. Ni/CeO_2 showed a higher CO_2 desorption temperature indicating that CeO_2 could provide stronger basic sites, which are beneficial for CO_2 adsorption and activation.

3.1.2. *Ni/support-CaO bifunctional combined materials*

The bifunctional combined materials (BCMs) for integrated CO_2 capture and reverse water–gas shift reaction (ICCU-RWGS) in this work were prepared by physically mixing the Ni/support catalysts and the sol–gel prepared CaO. As shown in Fig. 6a, 6b and 6c, the images of SEM and TEM were applied to exhibit the morphologies of sol–gel CaO and fresh Ni/CeO_2-CaO BCM. The sol–gel CaO adsorbent possessed a sponge-like structure with abundant large pores, consistent with the BET characterisation (Fig. 1 and Table 1). The porous structure could improve the CaO accessibility and prevent the severe sintering of CaO due to volume expansion during the carbonation process [36]. As shown in Fig. 6b, 6c and 6d, the physical mixing method could disperse Ni/CeO_2 into the sponge structure CaO, providing active sites near the adsorbent. In the previous research [32], the physical mixing method has been demonstrated to avoid the coverage of the catalytic sites caused by the volume expansion of CaO during the carbonation-hydrogenation ICCU process.

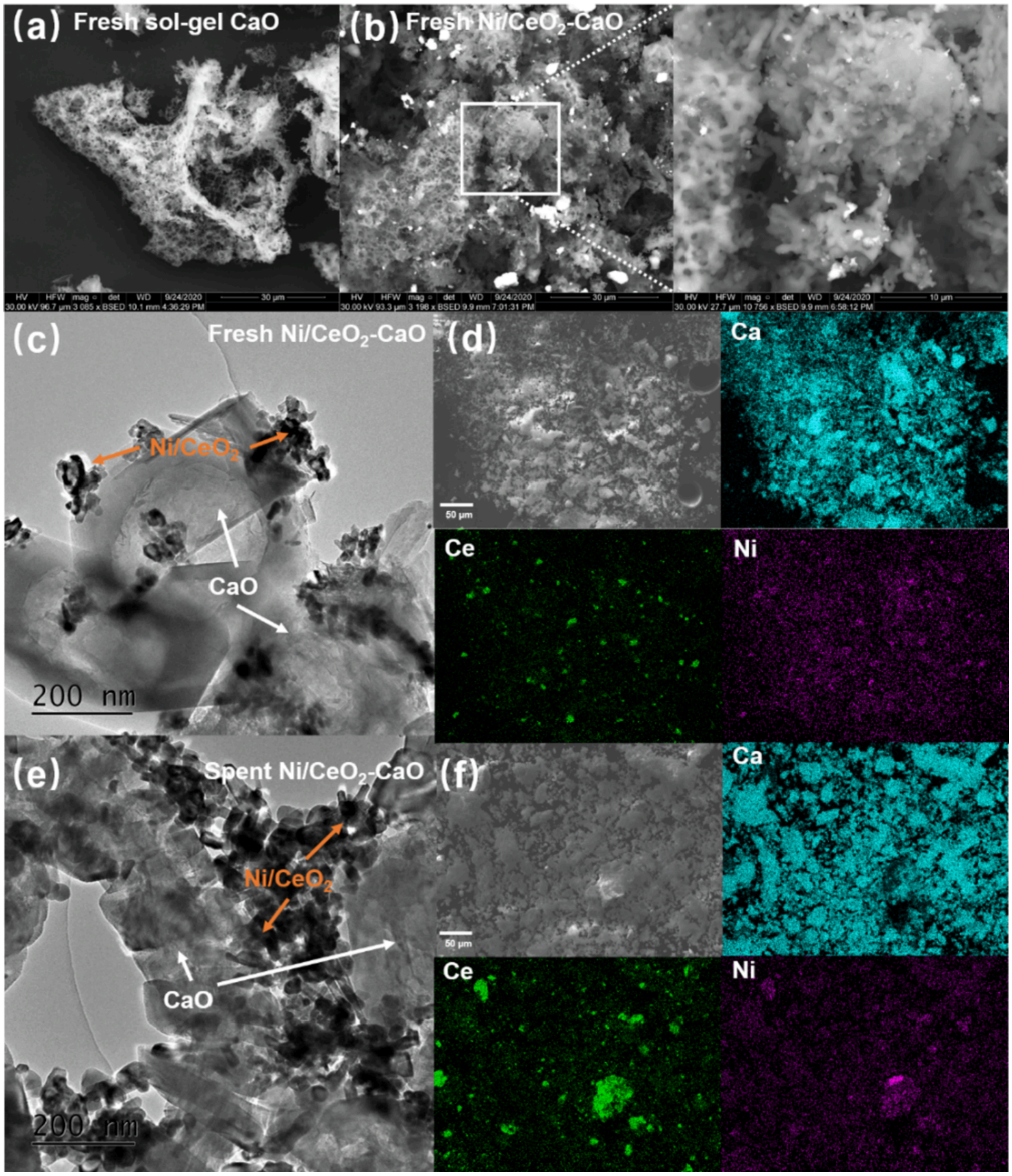

Fig. 6. SEM images of (a) fresh sol–gel CaO; (b) and (d) fresh Ni/CeO_2-CaO; (f) spent Ni/CeO_2-CaO; and TEM images of (c) fresh Ni/CeO_2-CaO and (e) spent Ni/CeO_2-CaO.

3.2. Integrated CO_2 capture and reverse water–gas shift reaction (ICCU-RWGS) performance

The ICCU-RWGS performance using Ni/support-CaO bifunctional combined materials (BCMs) with various supports (e.g. ZrO_2, TiO_2, CeO_2 and Al_2O_3) are shown in Fig. 7. Here Ni particles were used as active catalytic sites, and CaO played as the CO_2 adsorbent. A typical ICCU-RWGS process mainly included two steps, one was CO_2 adsorption from a diluted CO_2 source (e.g. 20% CO_2/N_2), and another was hydrogenation of the captured CO_2. The above two steps were isothermally operated by switching the inlet gas between 20% CO_2/N_2 and 5% H_2/N_2. The SiO_2/CaO was used as a blank benchmark material to demonstrate the ICCU-RWGS performance with bare inert support compared to active Ni metal over active supports. To reveal the optimal support for the ICCU-RWGS process, various Ni/support-CaO bifunctional combined materials were evaluated at 550–750 °C.

As shown in Fig. 7a and 7c, the CO_2 conversions and CO yields of various Ni/support-CaO BCMs followed the decreasing order: Ni/CeO_2-CaO > Ni/TiO_2-CaO > Ni/ZrO_2-CaO > Ni/Al_2O_3-CaO. All of the Ni/support-CaO BCMs exhibited excellent CO selectivity (~100%) over the investigated temperature range. The Ni/Al_2O_3-CaO showed only a comparable performance with SiO_2-CaO in terms of CO_2 conversion and CO yield, indicating the poor catalytic activities of nonreducible $NiAl_2O_4$ spinel (Fig. 5a). However, Ni/TiO_2-CaO with $NiTiO_3$ spinel achieved much high CO_2 conversion compared to Ni/Al_2O_3-CaO owing to the better spinel reducibility. Although there was no spinel formation, Ni/CeO_2-CaO outperforms Ni/ZrO_2-CaO in relation to CO_2 conversion and CO yield. For example, Ni/CeO_2-CaO and Ni/ZrO_2-CaO achieved 56.1% and 34.0% for CO_2 conversion and 2.7 and 1.1 mmol g^{-1} for CO yield at 650 °C, respectively.

The performances of ICCU-RWGS were also significantly affected by the reaction temperature. For example, 87.4% and 25.6% of CO_2 conversions were obtained over Ni/CeO_2-CaO at 550 °C and 750 °C, respectively. As an endothermic reaction, RWGS favors a higher reaction

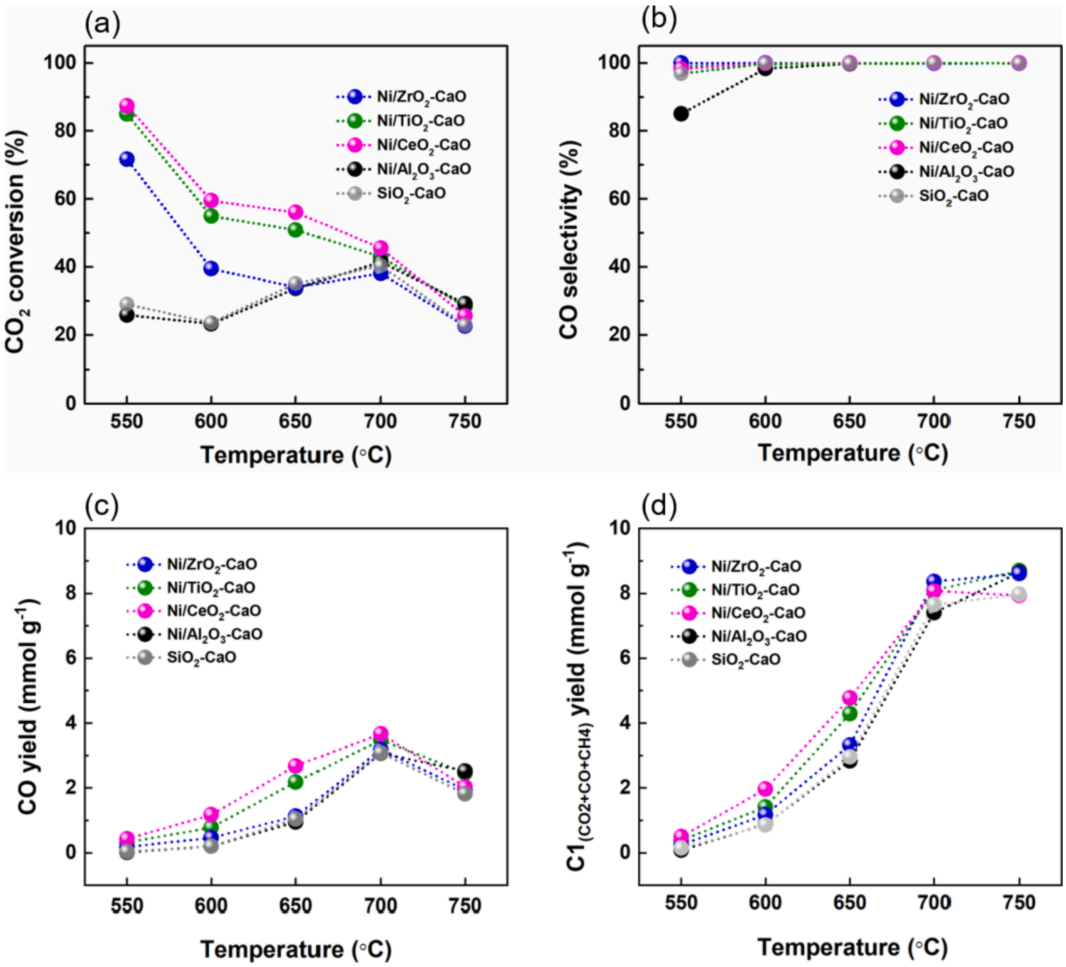

Fig. 7. Integrated CO_2 capture and RWGS performance of various Ni/support-CaO BCMs: (a) CO_2 conversion; (b) CO selectivity; (c) CO yield and (d) C1 species (CO_2 + CO + CH_4) yield.

temperature which is consistent with the decomposition of $CaCO_3$. However, the fast decomposition of $CaCO_3$ could increase the CO_2 concentration near the catalytic sites resulting in a decrease in CO_2 conversion.

It is necessary to monitor the real-time ICCU-RWGS process to evaluate the CO_2 adsorption performance and catalytic activity. The promotion effect of support of Ni could be clearly demonstrated in the CO_2 adsorption stage, presenting as the enhanced CO_2 capture rate compared to the benchmark (SiO_2 line in Fig. 8a). Specifically, Ni/CeO_2-CaO and Ni/Al_2O_3-CaO exhibited superior CO_2 capture rate and capacity (~9.58 and 9.31 mmol g-1 at 650 °C for ~28 min), which was attributed to the abundant basicity of Ni/CeO_2 and Ni/Al_2O_3, as indicated in Fig. 5b.

The various Ni/support-CaO BCMs also exhibited distinct CO generation rates and real-time CO_2 conversion during the hydrogenation step. As shown in Fig. 8b and 8c, the Ni/CeO_2-CaO BCM could achieve an optimal real-time CO_2 conversion (~60%) and CO generation rate (~1.7 μmol $s^{-1}g^{-1}$) at 650 °C. The excellent Ni dispersion and stronger basicity of Ni/CeO_2 might contribute to the superior ICCU-RWGS performance. It is worth noting that Ni/TiO_2-CaO also exhibited outstanding real-time CO_2 conversion (~57%), which might be attributed to the slowly released Ni from easily reducible $NiTiO_3$ spinel species (Figs. 3 and 4) [50]. As a comparison, Ni/Al_2O_3 showed poorer catalytic activities, indicating that the nonreducible spinel (Figs. 3 and 4a) played poor catalytic performance in ICCU.

In this work, we focused on the initial 1500 s of CO_2 conversion to evaluate the real-time gas production in ICCU-RWGS. The CO_2 desorption is relatively fast in the initial stage of the hydrogenation step (0–500 s), especially under higher temperature (e.g. 700 °C), which directly limits the CO_2 conversion rate at this stage (as shown in Fig. 8e and 8f). Since only 5% H_2/N_2 was used in this work, excessive CO_2 release would decrease the ratio of H_2:CO_2 and affect the equilibrium of RWGS reaction. After the rapid decomposition of the surface layer of $CaCO_3$, the release of CO_2 and the performance of RWGS is gradually stabilised until the carbonates are thoroughly consumed.

The scaled-up preparation of Ni/supports-CaO BCM is critical for deploying the ICCU-RWGS in an industrial scale. The adsorbents (CaO) are expected to be obtained from limestones, representing a low-cost mineral (<30 dollars per ton (DPT)). The Ni/supports are comprised of earth-rich elements, such as CeO_2 (~1600 DPT), TiO_2 (~3300 DPT), Al_2O_3 (~350 DPT), ZrO_2 (~1000 DPT) and Ni precursor (Ni $(NO_3)_2$*xH_2O, ~4000 DPT). By impregnating Ni onto a support and physically mixing catalysts and CaO, the BCMs could be obtained with an expected cost of ~300–1000 DPT. Notably, although H_2 can be obtained from renewable energy, the cost would dominate in the ICCU-RWGS process. The development of low-cost hydrogen production will also be the key to the low-cost deployment of ICCU.

3.3. ICCU-RWGS cycle evaluation

The stability of Ni/CeO_2-CaO bifunctional combined material was presented by carrying out 20 cycles of ICCU-RWGS at 650 °C (Fig. 9). The Ni/CeO_2-CaO possessed a < 5% decrease for CO and C1 yield (CO_2 + CO + CH_4) and > 99% CO selectivity after 20 cycles, indicating

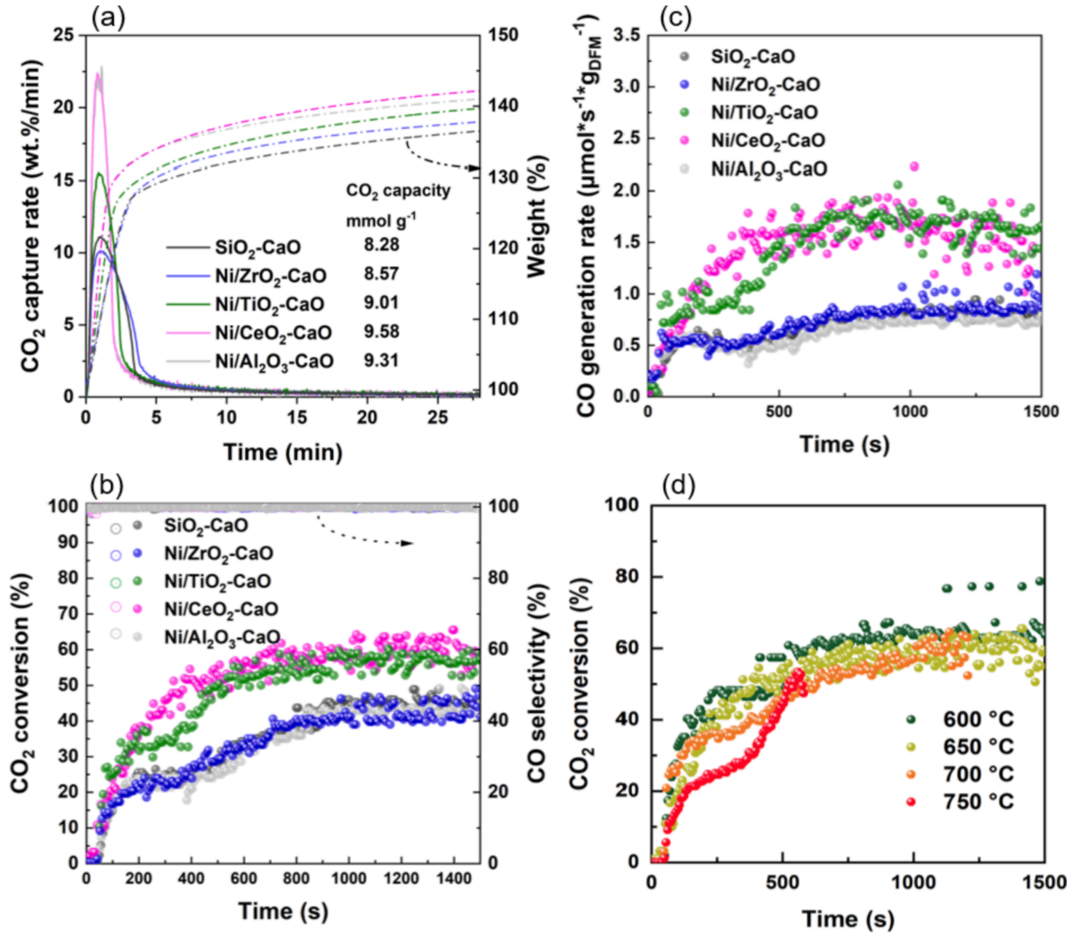

Fig. 8. Real-time performance of various Ni/support-CaO BCMs over ICCU-RWGS at 650 °C: (a) CO_2 capture performance collected on TGA; (b) CO_2 conversion and CO selectivity; (c) CO generation rate and CO_2 conversion (d) under various temperature over Ni/CeO_2-CaO.

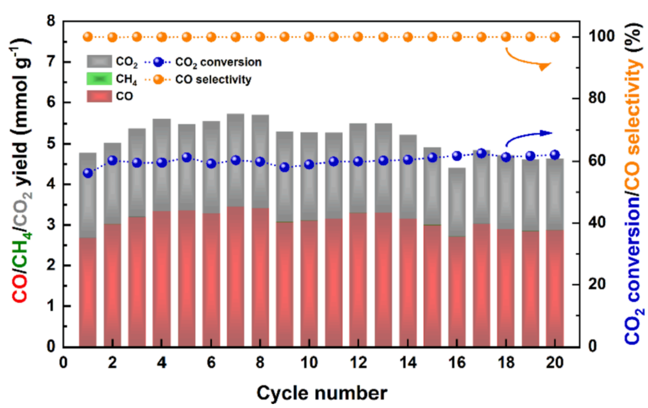

Fig. 9. Cycle performance of Ni/CeO_2-CaO over ICCU-RWGS at 650 °C.

the excellent and stable ICCU-RWGS performance. Notably, the overall CO_2 conversion slightly increased from 56.07% in the 1st cycle to 62.03% in the 20th cycle, which outperforms the state-of-art ICCU-RWGS performance using similar conditions (Table 2). It is believed that the effective reactant spillover onto catalytic sites is critical in the catalytic process [51]. As shown in Fig. 6e, Ni/CeO_2 and CaO exhibited closer contact in spent Ni/CeO_2-CaO, indicating a shorter CO_2 spillover distance. The self-optimisation of Ni/CeO_2-CaO bifunctional combined material in ICCU-RWGS might be attributed to the volume expansion–shrinkage effect of the sol–gel CaO in cyclic carbonation-hydrogenation, which partially embedded Ni/CeO_2 onto the surface layer of CaO.

4. Conclusions

In this work, several Ni/support-CaO bifunctional combined materials (BCMs) were prepared by physically mixing sol–gel CaO and Ni catalysts with various supports (ZrO_2, TiO_2, CeO_2 and Al_2O_3). The CO_2 adsorption and catalytic performance of Ni/support-CaO BCMs were evaluated via integrated CO_2 capture and reverse water–gas shift (ICCU-RWGS) process at different temperatures from 550 to 750 °C. The Ni/CeO_2-CaO outperformed the other Ni/support-CaO (support = ZrO_2, TiO_2 or Al_2O_3) over ICCU-RWGS performance (CO_2 adsorption and catalytic activity). The enhanced CO_2 adsorption performance was attributed to the stronger basicity of Ni/Al_2O_3 and Ni/CeO_2. And the improved catalytic performance (CO_2 conversion, CO yield and CO generate rate) was related to the excellent Ni dispersion and reducibility. The spinel formation contributed to the Ni species dispersion by forming strong interaction with support; however, only the easy-reducible spinel ($NiTiO_3$) was active in the ICCU process. Furthermore, the Ni/CeO_2-CaO exhibited excellent stability in 20 cycles of ICCU and showed a self-optimising trend in CO_2 conversion (56.07% and 62.03% for the 1st and 20th cycles, respectively) due to the gradually close distance between CaO and Ni/CeO_2 owing to the volume expansion and shrinkage of CaO during carbonation-hydrogenation cycles.

CRediT authorship contribution statement

Shuzhuang Sun: Conceptualization, Methodology, Formal analysis,

Table 2
Comparison of ICCU-RWGS performance of Ni/CeO_2-CaO and materials from literature.

Materials	Mixture method	ICCU condition	CO_2 capacity	CO_2 conv.	CO sel.	Cycle stability	Ref.
Ni/CeO_2-CaO (~3.3% Ni)	Physical mixture	Adsorption: 650 °C, 20% CO_2/N_2 Hydrogenation: 650 °C, 5% H_2/N_2	9.6	62%	100%	20	This work
Ni/$CeCaCO_3$	impregnation	Adsorption: 550 °C, 20% CO_2/N_2 Hydrogenation: 550 °C, 5% H_2/N_2	10.0	42%	26%	n.a.	[32]
1 %NiCaO	One-pot	Same as above	9.2	38%	42%	n.a.	[32]
10 %NiCaO	One-pot	Same as above	8.1	45%	31%	n.a.	[32]
Ni/CS	wet-mixing	Adsorption: 650 °C, 10% CO_2/N_2 Hydrogenation: 650 °C, 5% H_2/N_2	3.6	21.9%	n.a.	5	[25]
Ni/CS-P30	Impregnation	Same as above	8.4	34%	n.a.	5	[25]
Ni/CS-P30-C	Impregnation	Same as above	13.3	39%	n.a.	5	[25]
$Ca_1Ni_{0.1}$	One-pot	Adsorption: 650 °C, 15% CO_2/N_2 Hydrogenation: 650 °C, 5% H_2/N_2	15.0	46%	n.a.	20	[20]
$Ca_1Ni_{0.1}Ce_{0.017}$	One-pot	Same as above	14.2	51%	n.a.	n.a.	[20]
$Ca_1Ni_{0.1}Ce_{0.033}$	One-pot	Same as above	14.1	52%	n.a.	20	[20]

Investigation, Data curation, Writing – original draft. **Chen Zhang:** Methodology, Investigation, Formal analysis. **Shaoliang Guan:** Formal analysis, Investigation, Resources. **Shaojun Xu:** Formal analysis, Resources, Writing – review & editing, Supervision. **Paul T. Williams:** Formal analysis, Resources, Writing – review & editing, Supervision. **Chunfei Wu:** Conceptualization, Writing – review & editing, Supervision, Project administration, Funding acquisition.

Declaration of Competing Interest

The authors declare that they have no known competing financial interests or personal relationships that could have appeared to influence the work reported in this paper.

Acknowledgements

The authors gratefully acknowledge financial support from the China Scholarship Council (reference number: 201906450023). This project has received funding from the European Union's Horizon 2020 research and innovation programme under the Marie Skłodowska-Curie grant agreement No 823745. The UK Catalysis Hub is kindly thanked for the resources and support provided via our membership of the UK Catalysis Hub Consortium and funded by EPSRC grant: EP/R026939/1, EP/R026815/1, EP/R026645/1, EP/R027129/1 or EP/M013219/1(biocatalysis). The XPS data collection was performed at the EPSRC National Facility for XPS ('HarwellXPS'), operated by Cardiff University and UCL, under contract No. PR16195.

References

[1] M.D. Garba, M. Usman, S. Khan, F. Shehzad, A. Galadima, M.F. Ehsan, A. S. Ghanem, M. Humayun, CO_2 towards fuels: A review of catalytic conversion of carbon dioxide to hydrocarbons, J. Environ. Chem. Eng. 9 (2020) 104756, https://doi.org/10.1016/j.jece.2020.104756.

[2] G.L. Foster, E.J. Rohling, Relationship between sea level and climate forcing by CO_2 on geological timescales, Proc. Natl. Acad. Sci. 110 (2013) 1209–1214, https://doi.org/10.1073/pnas.1216073110.

[3] F. Melzner, F.C. Mark, B.A. Seibel, L. Tomanek, Ocean acidification and coastal marine invertebrates: tracking CO_2 effects from seawater to the cell, Ann. Rev. Mar. Sci. 12 (2020) 499–523, https://doi.org/10.1146/annurev-marine-010419-010658.

[4] C. Liu, Y.O. Susilo, A. Karlström, Estimating changes in transport CO_2 emissions due to changes in weather and climate in Sweden, Transport. Res. Part D: Trans. Environ. 49 (2016) 172–187, https://doi.org/10.1016/j.trd.2016.09.004.

[5] Y. Guo, J. Sun, R. Wang, W. Li, C. Zhao, C. Li, J. Zhang, Recent advances in potassium-based adsorbents for CO_2 capture and separation: a review, Carbon Capture Sci. Technol. 1 (2021) 100011, https://doi.org/10.1016/j.ccst.2021.100011.

[6] J. Buckingham, T.R. Reina, M.S. Duyar, Recent advances in carbon dioxide capture for process intensification, Carbon Capture Sci. Technol. 2 (2022) 100031, https://doi.org/10.1016/j.ccst.2022.100031.

[7] W.Y. Hong, A techno-economic review on carbon capture, utilisation and storage systems for achieving a net-zero CO_2 emissions future, Carbon Capture Sci. Technol. 3 (2022) 100044, https://doi.org/10.1016/j.ccst.2022.100044.

[8] Y. Qiao, J.J. Bailey, Q. Huang, X. Ke, C. Wu, Potential photo-switching sorbents for CO_2 capture–A review, Renew. Sustain. Energy Rev. 158 (2022) 112079, https://doi.org/10.1016/j.rser.2022.112079.

[9] T.N. Borhani, M. Wang, Role of solvents in CO_2 capture processes: The review of selection and design methods, Renew. Sustain. Energy Rev. 114 (2019) 109299, https://doi.org/10.1016/j.rser.2019.109299.

[10] T. Luo, C. Luo, Z. Shi, X. Li, F. Wu, L. Zhang, Optimization of sol-gel combustion synthesis of calcium looping CO_2 sorbents, Part II: Effects of thermal activation conditions, Sep. Purif. Technol. 292 (2022) 121061, https://doi.org/10.1016/j.seppur.2022.121061.

[11] T. Luo, C. Luo, Z. Shi, X. Li, F. Wu, L. Zhang, Optimization of sol-gel combustion synthesis for calcium looping CO_2 sorbents, Part I: Effects of sol-gel preparation and combustion conditions, Sep. Purif. Technol. 292 (2022) 121081, https://doi.org/10.1016/j.seppur.2022.121081.

[12] J. Chen, L. Duan, Z. Sun, Review on the development of sorbents for calcium looping, Energy Fuels 34 (2020) 7806–7836, https://doi.org/10.1021/acs.energyfuels.0c00682.

[13] D.P. Hanak, S. Michalski, V. Manovic, From post-combustion carbon capture to sorption-enhanced hydrogen production: A state-of-the-art review of carbonate looping process feasibility, Energy Convers. Manage. 177 (2018) 428–452, https://doi.org/10.1016/j.enconman.2018.09.058.

[14] D. Leeson, N. Mac Dowell, N. Shah, C. Petit, P. Fennell, A Techno-economic analysis and systematic review of carbon capture and storage (CCS) applied to the iron and steel, cement, oil refining and pulp and paper industries, as well as other high purity sources, Int. J. Greenhouse Gas Control 61 (2017) 71–84, https://doi.org/10.1016/j.ijggc.2017.03.020.

[15] H.-J. Ho, A. Iizuka, E. Shibata, Carbon capture and utilization technology without carbon dioxide purification and pressurization: a review on its necessity and available technologies, Ind. Eng. Chem. Res. 58 (2019) 8941–8954, https://doi.org/10.1021/acs.iecr.9b01213.

[16] S. Sun, H. Sun, P.T. Williams, C. Wu, Recent advances in integrated CO_2 capture and utilization: a review, Sustain. Energy Fuels 5 (2021) 4546–4559, https://doi.org/10.1039/D1SE00797A.

[17] H. Sun, Y. Zhang, S. Guan, J. Huang, C. Wu, Direct and highly selective conversion of captured CO_2 into methane through integrated carbon capture and utilization over dual functional materials, J. CO_2 Utili. 38 (2020) 262–272, https://doi.org/10.1016/j.jcou.2020.02.001.

[18] A. Bermejo-López, B. Pereda-Ayo, J.A. Onrubia-Calvo, J.A. González-Marcos, J. R. González-Velasco, Tuning basicity of dual function materials widens operation temperature window for efficient CO_2 adsorption and hydrogenation to CH_4, J. CO_2 Utiliz. 58 (2022) 101922, https://doi.org/10.1016/j.jcou.2022.101922.

[19] S. Sun, H. Sun, S. Guan, S. Xu, C. Wu, Integrated CO_2 capture and methanation on Ru/CeO_2-MgO combined materials: Morphology effect from CeO_2 support, Fuel 317 (2022) 123420, https://doi.org/10.1016/j.fuel.2022.123420.

[20] H. Sun, J. Wang, J. Zhao, B. Shen, J. Shi, J. Huang, C. Wu, Dual functional catalytic materials of Ni over Ce-modified CaO sorbents for integrated CO_2 capture and conversion, Appl. Catal. B: Environ. 244 (2019) 63–75.

[21] R.B. Anderson, Fischer-Tropsch Synthesis, Academic Press Inc., United Kingdom, 1984.

[22] S. Sun, Z. Lv, Y. Qiao, C. Qin, S. Xu, C. Wu, Integrated CO_2 capture and utilization with CaO-alone for high purity syngas production, Carbon Capture Sci. Technol. 1 (2021) 100001, https://doi.org/10.1016/j.ccst.2021.100001.

[23] S. Sun, S. He, C. Wu, Ni promoted Fe-CaO dual functional materials for calcium chemical dual looping, Chem. Eng. J. 441 (2022) 135752, https://doi.org/10.1016/j.cej.2022.135752.

[24] A. Mustafa, B.G. Lougou, Y. Shuai, Z. Wang, H. Tan, Current technology development for CO_2 utilization into solar fuels and chemicals: A review, J. Energy Chem. 49 (2020) 96–123, https://doi.org/10.1016/j.jechem.2020.01.023.

[25] G. Wang, Y. Guo, J. Yu, F. Liu, J. Sun, X. Wang, T. Wang, C. Zhao, Ni-CaO dual function materials prepared by different synthetic modes for integrated CO_2 capture and conversion, Chem. Eng. J. 428 (2022) 132110, https://doi.org/10.1016/j.cej.2021.132110.

[26] L.F. Bobadilla, J.M. Riesco-García, G. Penelás-Pérez, A. Urakawa, Enabling continuous capture and catalytic conversion of flue gas CO_2 to syngas in one

process, J. CO_2 Utiliz. 14 (2016) 106–111, https://doi.org/10.1016/j.jcou.2016.04.003.
[27] B. Shao, G. Hu, K.A. Alkebsi, G. Ye, X. Lin, W. Du, J. Hu, M. Wang, H. Liu, F. Qian, Heterojunction-redox catalysts of $Fe_xCo_yMg_{10}CaO$ for high-temperature CO_2 capture and in situ conversion in the context of green manufacturing, Energy Environ. Sci. 14 (2021) 2291–2301, https://doi.org/10.1039/D0EE03320K.
[28] H. Sun, J. Wang, X. Liu, B. Shen, C.M. Parlett, G.O. Adwek, E.J. Anthony, P. T. Williams, C. Wu, Fundamental studies of carbon capture using CaO-based materials, J. Mater. Chem. A 7 (2019) 9977–9987, https://doi.org/10.1039/C8TA10472G.
[29] J. Hu, P. Hongmanorom, V.V. Galvita, Z. Li, S. Kawi, Bifunctional Ni-Ca based material for integrated CO2 capture and conversion via calcium-looping dry reforming, Appl. Catal. B: Environ. 284 (2021) 119734.
[30] C. Alvarez-Galvan, J.L. Martínez, M. Capel-Sanchez, L. Pascual, J.A. Alonso, Magnetic properties of efficient catalysts based on La-doped ceria-supported nickel nanoparticles for rWGS reaction. Influence of Ni Loading, Adv. Sustain. Syst. 5 (2021) 2100029, https://doi.org/10.1002/adsu.202100029.
[31] X. Su, X. Yang, B. Zhao, Y. Huang, Designing of highly selective and high-temperature endurable RWGS heterogeneous catalysts: recent advances and the future directions, J. Energy Chem. 26 (2017) 854–867, https://doi.org/10.1016/j.jechem.2017.07.006.
[32] H. Sun, Y. Wang, S. Xu, A.I. Osman, G. Stenning, J. Han, S. Sun, D. Rooney, P. T. Williams, F. Wang, C. Wu, Understanding the interaction between active sites and sorbents during the integrated carbon capture and utilization process, Fuel 286 (2021) 119308, https://doi.org/10.1016/j.fuel.2020.119308.
[33] J. Barbero, M. Peña, J. Campos-Martin, J. Fierro, P. Arias, Support effect in supported Ni catalysts on their performance for methane partial oxidation, Catal. Lett. 87 (2003) 211–218, https://doi.org/10.1023/A:1023407609626.
[34] J.W. Han, J.S. Park, M.S. Choi, H. Lee, Uncoupling the size and support effects of Ni catalysts for dry reforming of methane, Appl. Catal. B: Environ. 203 (2017) 625–632, https://doi.org/10.1016/j.apcatb.2016.10.069.
[35] V. Shanmugam, S. Neuberg, R. Zapf, H. Pennemann, G. Kolb, Effect of support and chelating ligand on the synthesis of Ni catalysts with high activity and stability for CO_2 methanation, Catalysts 10 (2020) 493, https://doi.org/10.3390/catal10050493.
[36] E. Santos, C. Alfonsín, A. Chambel, A. Fernandes, A.S. Dias, C. Pinheiro, M. Ribeiro, Investigation of a stable synthetic sol–gel CaO sorbent for CO_2 capture, Fuel 94 (2012) 624–628.
[37] T. Montini, M. Melchionna, M. Monai, P. Fornasiero, Fundamentals and catalytic applications of CeO_2-based materials, Chem. Rev. 116 (2016) 5987–6041.
[38] A. Mazhar, A.H. Khoja, A.K. Azad, F. Mushtaq, S.R. Naqvi, S. Shakir, M. Hassan, R. Liaquat, M. Anwar, Performance analysis of TiO_2-modified Co/$MgAl_2O_4$ catalyst for dry reforming of methane in a fixed bed reactor for syngas (H_2, CO) production, Energies 14 (2021) 3347.
[39] S. Zhang, M. Ying, J. Yu, W. Zhan, L. Wang, Y. Guo, Y. Guo, $Ni_xAl_1O_{2-\delta}$ mesoporous catalysts for dry reforming of methane: The special role of $NiAl_2O_4$ spinel phase and its reaction mechanism, Appl. Catal. B: Environ. 291 (2021) 120074.
[40] K. Lopes, L. Cavalcante, A.Z. Simões, J.A. Varela, E. Longo, E. Leite, $NiTiO_3$ powders obtained by polymeric precursor method: Synthesis and characterization, J. Alloy. Compd. 468 (2009) 327–332.
[41] D. Hu, C. Liu, L. Li, K.-L. Lv, Y.-H. Zhang, J.-L. Li, Carbon dioxide reforming of methane over nickel catalysts supported on TiO_2 (001) nanosheets, Int. J. Hydrogen Energy 43 (2018) 21345–21354, https://doi.org/10.1016/j.ijhydene.2018.09.188.
[42] N. Sahli, C. Petit, A.-C. Roger, A. Kiennemann, S. Libs, M.M. Bettahar, Ni catalysts from $NiAl_2O_4$ spinel for CO_2 reforming of methane, Catal. Today 113 (2006) 187–193, https://doi.org/10.1016/j.cattod.2005.11.065.
[43] H. Nesbitt, D. Legrand, G. Bancroft, Interpretation of Ni2p XPS spectra of Ni conductors and Ni insulators, Phys. Chem. Miner. 27 (2000) 357–366.
[44] A.L. Luna, D. Dragoe, K. Wang, P. Beaunier, E. Kowalska, B. Ohtani, D. Bahena Uribe, M.A. Valenzuela, H. Remita, C. Colbeau-Justin, Photocatalytic hydrogen evolution using Ni–Pd/TiO_2: correlation of light absorption, charge-carrier dynamics, and quantum efficiency, J. Phys. Chem. C 121 (2017) 14302–14311.
[45] S. Lin, Z. Hao, J. Shen, X. Chang, S. Huang, M. Li, X. Ma, Enhancing the CO_2 methanation activity of Ni/CeO_2 via activation treatment-determined metal-support interaction, J. Energy Chem. 59 (2021) 334–342.
[46] M. Peymani, S.M. Alavi, H. Arandiyan, M. Rezaei, Rational design of high surface area mesoporous Ni/CeO_2 for partial oxidation of propane, Catalysts 8 (2018) 388, https://doi.org/10.3390/catal8090388.
[47] T.A. Le, M.S. Kim, S.H. Lee, T.W. Kim, E.D. Park, CO and CO_2 methanation over supported Ni catalysts, Catal. Today 293 (2017) 89–96, https://doi.org/10.1016/j.cattod.2016.12.036.
[48] Z. Boukha, C. Jiménez-González, B. de Rivas, J.R. González-Velasco, J.I. Gutiérrez-Ortiz, R. López-Fonseca, Synthesis, characterisation and performance evaluation of spinel-derived Ni/Al_2O_3 catalysts for various methane reforming reactions, Appl. Catal. B: Environ. 158 (2014) 190–201, https://doi.org/10.1016/j.apcatb.2014.04.014.
[49] A.H. Fakeeha, M.A. Naeem, W.U. Khan, A.E. Abasaeed, A.S. Al-Fatesh, Reforming of methane by CO_2 over bimetallic Ni-Mn/γ-Al_2O_3 catalyst, Chin. J. Chem. Phys. 27 (2014) 214, https://doi.org/10.1063/1674-0068/27/02/214-220.
[50] J. Ye, Y. Wang, Y. Liu, H. Wang, Steam reforming of ethanol over Ni/$CexTi_{1-x}O_2$ catalysts, Int. J. Hydrogen Energy 33 (2008) 6602–6611, https://doi.org/10.1016/j.ijhydene.2008.08.036.
[51] W.C. Conner Jr, J.L. Falconer, Spillover in heterogeneous catalysis, Chem. Rev. 95 (1995) 759–788, https://doi.org/10.1021/cr00035a014.